

Frequency-selective effective model of driven multilevel systems in gate-defined quantum dots

Yuan Zhou,^{1,2} Sisi Gu,^{1,2} Ke Wang,^{1,2} Gang Cao,^{1,2} Xuedong Hu,³ Ming Gong,^{1,2,*} Hai-Ou Li,^{1,2,†} and Guo-Ping Guo^{1,2,4,‡}

¹CAS Key Laboratory of Quantum Information, University of Science and Technology of China, Hefei, Anhui 230026, China

²CAS Center for Excellence and Synergetic Innovation Center in Quantum Information and Quantum Physics, University of Science and Technology of China, Hefei, Anhui 230026, China

³Department of Physics, University at Buffalo, SUNY, Buffalo, New York 14260, USA

⁴Origin Quantum Computing Company Limited, Hefei, Anhui 230026, China

(Dated: October 20, 2021)

Landau-Zener-Stückelberg (LZS) interference is a common tool to study various quantum systems. When system is driven forth and back through anticrossings, phases are accumulated coherently, and results in constructive or destructive interference. LZS are widely demonstrated in two-level systems and multilevel systems. Nonetheless, multilevel physics in LZS interference of a multilevel system remains unexplored, since in most of the cases, influence of each anticrossing can be treated separately, thus two-level model is sufficient. Here, we investigate the LZS interference of multilevel systems in quantum dots (QDs), and propose a scheme to realize an effective model from the complicated energy levels. By employing this model, we study the physics in multilevel system such as Autler-Townes splitting (ATS), electromagnetically induced transparency and coherent population trapping (CPT) *etc.*, and reveal their unique behaviors in our scheme. Specifically, possible improvement for present two-qubit gate in QDs and noise-robust quantum gates are proposed. The theoretical consideration we present is rather general, and thus is in principle valid for other quantum systems with the similar energy structure.

I. INTRODUCTION

Multilevel systems are ubiquitous in quantum systems, and have been studied extensively in varieties of systems. Based on driving fields, phenomena in multilevel systems such as ATS [1–3], electromagnetically induced transparency, CPT [4–10] and stimulated Raman by adiabatic passage [11–14] have been demonstrated. These phenomena are the major theme in the textbooks of quantum optics [15], and importantly, weak transversely driving fields are required in these experiments. Another important phenomena of driven system is LZS interference, which only requires a strong longitudinal drive [16, 17]. Among the common quantum systems, artificial quantum systems take the advantage of excellent tunability, strong longitudinal drive is more feasible, thus LZS is widely demonstrated in these systems. For example, LZS interference has been demonstrated in artificial quantum systems such as superconducting circuit [18–20], gate-defined QDs [21–23], nitrogen-vacancy color centers [24]. However, multilevel physics in LZS interference of multilevel system has received less attention. Though implemented with a multilevel system, some results can be well characterized by effective two-level models [23, 25, 26], or by treating anticrossings separately [19], which is essentially two-level model. Other literatures interpret their result by means of numerical simulation [27] or approx-

imated based on additional assumptions [28], where the basic physics is obscured.

Gate-defined QDs as one of the artificial quantum systems has been proved as a valid candidate for quantum computation and quantum simulation. Comparing to other quantum systems, gate-defined QDs system has the advantage of highly integration, all-electric manipulation, well controlled geometries by the semiconductor lithography techniques and high manipulation temperature [29–31]. In addition, transversely driving in QDs system is sometimes challenging since the off-diagonal elements in Hamiltonian is not always tunable, whereas diagonal elements can be tuned conveniently. Hence, LZS is an important topic in QDs, which has been applied to qubit manipulation [21], dephasing characterizing [23], spectroscopy [22] *et al.*

Here, we study two typical longitudinally driven multilevel systems in QDs, and a three-level effective model is derived, which provides an insight into the multilevel LZS process. Based on the three-level model, various multilevel physics can be studied. Comparing to previous works where the multilevel structure is treated as sequential two-level structures, physics in the three-level effective model is distinctive. When two-level LZS is considered, the coherent phase dominates the physics. In contrast, in multilevel systems, when several paths exist simultaneously, interference between phases of different paths happens, which brings out multilevel physics. The effective model can be determined by driving frequency and tuned by driving amplitude. With this approach, we demonstrate several celebrated schemes, including ATS, CPT and state transfer via adiabatic passage, which are quite different from the common ones. This proposal

* gongm@ustc.edu.cn

† haiouli@ustc.edu.cn

‡ gpguo@ustc.edu.cn

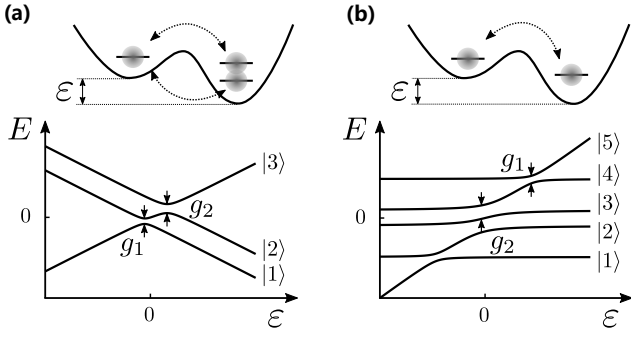


FIG. 1. **Gate-defined QDs and their lowest energy levels.** (a) Realization of the three-level model based on hybrid qubit with three spins. (b) Realization of the five-level model based on singlet-triplet qubit system using two spins. In these systems, the off-diagonal couplings g_i between different states are realized based on tunneling through the barrier and spin-orbit coupling, while the energies in the diagonal terms can be tuned by the detuning between the two quantum dots, denoted by ε throughout this manuscript.

enables the applications of LZS in quantum computation and quantum simulation, and potentially broaden the capacity of QDs in their future applications.

II. MULTILEVEL MODELS AND EFFECTIVE HAMILTONIAN

We consider the physics in two coupled gate-defined QDs with charge and spin configurations as shown in Fig. 1 (a), (b), and mainly consider two most relevant schemes studied in recent experiments using coupled QDs. In the hybrid qubit system [32–35] shown in 1 (a), which is described by the three-level model. In the subspace with total spin $S = 1/2$ and $S_z = -1/2$, the lowest three-levels can be isolated from the excited manifolds, yielding the following basis [32, 36]

$$\begin{aligned} |1\rangle &= |\downarrow, S\rangle, & |2\rangle &= \sqrt{\frac{1}{3}}|\downarrow, T_0\rangle - \sqrt{\frac{2}{3}}|\uparrow, T_-\rangle, \\ |3\rangle &= |S, \downarrow\rangle, \end{aligned} \quad (1)$$

where $|S\rangle = (|\uparrow\downarrow\rangle - |\downarrow\uparrow\rangle)/\sqrt{2}$, $|T_0\rangle = (|\uparrow\downarrow\rangle + |\downarrow\uparrow\rangle)/\sqrt{2}$ and $|T_-\rangle = |\downarrow\downarrow\rangle$ are the singlet and triplet states in the right dot. In this model, both couplings labeled by g_1 , g_2 are determined by the inter-dot tunneling (typically about 2 – 5 GHz [34]). The five-level structure in Fig. 1 (b) is also widely explored based on singlet-triplet (ST) system [37–42], which has been employed to demonstrate spin-based two-qubit gate with gate fidelity of 98% [40]. The basis of ST system is given by

$$\begin{aligned} |1\rangle &= |\uparrow, \uparrow\rangle, & |2\rangle &= |\uparrow, \downarrow\rangle, & |3\rangle &= |\downarrow, \uparrow\rangle, \\ |4\rangle &= |\downarrow, \downarrow\rangle, & |5\rangle &= |S, 0\rangle. \end{aligned} \quad (2)$$

In ST system, the coupling denoted by g_2 (couplings between $|2\rangle$, $|3\rangle$ and $|5\rangle$) is proportional to the inter-dot

tunneling, while g_1 (couplings between $|1\rangle$, $|4\rangle$ and $|5\rangle$) is induced by the spin-orbit interaction with spin flip during tunneling, which can not be tuned conveniently. Hereafter, state $|3\rangle$ in Eq. 1 and $|5\rangle$ in Eq. 2 will be termed as the shuttle state. These states response differently to the gate voltage detuning ε for their different charge configurations as is shown in Fig. 1, and consequently can be detected directly via electrical method. Relevant parameters of hybrid and ST system are summarized in Table I in Appendix. A.

Our central idea is to realize a three-level effective models from these driven levels, which can be illustrated using the model in Fig. 1 (a)

$$H(t) = \begin{pmatrix} E_1 & 0 & g_1 \\ 0 & E_2 & g_2 \\ g_1 & g_2 & \tilde{E}_3(t) \end{pmatrix}, \quad (3)$$

where $\tilde{E}_3(t) = E_3 - A \cos(\omega t)$ is the longitudinal driving field, setting $\hbar = 1$. To achieve the effective Hamiltonian, we need to first eliminate the longitudinal field by $\mathcal{U} = \text{diag}(e^{i(E_2+n\omega)t}, e^{iE_2t}, e^{i\int_0^t d\tau E_3(\tau)+\delta})$, where $\delta \equiv E_2 - E_3 + N\omega$ is a frequency offset. The offset δ not only ensures the translation symmetry of $\tilde{H}(t) = \tilde{H}(t+T)$, but also keep the diagonal term in the first Brillouin zone. Then the equivalent model is given by $\tilde{H}(t) = \mathcal{U}^\dagger H(t) \mathcal{U} - i\mathcal{U}^\dagger \partial_t \mathcal{U}$. From \tilde{H} we obtain the effective Hamiltonian by performing the Floquet expansion [43] followed by a Schrieffer-Wolff (SW) transformation [44]. Details are presented in Appendix. B.

The effective Hamiltonian is obtained as

$$H_{\text{eff}} = \begin{pmatrix} E_{12} - n\omega + \Delta' & \xi & g_1 J_{N-n} \\ \xi^* & \Delta & g_2 J_N \\ g_1^* J_{N-n} & g_2^* J_N & -\delta - \Delta - \Delta' \end{pmatrix}, \quad (4)$$

with $E_{ij} = E_i - E_j$ and $J_k = J_k(\frac{A}{\omega})$ being first-kind Bessel function of the k -th order and Δ' , Δ , ξ are corrections arising from second-order SW transformation (see Appendix. B3). This is equivalent to the effective Hamiltonian given by Magnus expansion [45] when $E_{12} = n\omega$ and $E_{32} = N\omega$, nonetheless, Eq. 4 is efficient in a broader regime. The effective model shows that by modulating the diagonal term, all the off-diagonal couplings can be tuned accordingly. Specifically, a synthetic coupling labeled by ξ is generated. This kind of tunability is a rather trivial issue in atoms and some artificial atoms, where couplings can be controlled by driving field amplitude individually; however, it is non-trivial in hybrid/ST system since g_1 , g_2 is challenging to couple to driving field individually in practice.

III. ATS INDUCED BY LONGITUDINAL DRIVE

The amplitude spectrum manifest some characteristic phenomena due to the modulation on diagonal elements. We present a full calculation of $H(t)$ with $g_1 = 0.1$ GHz,

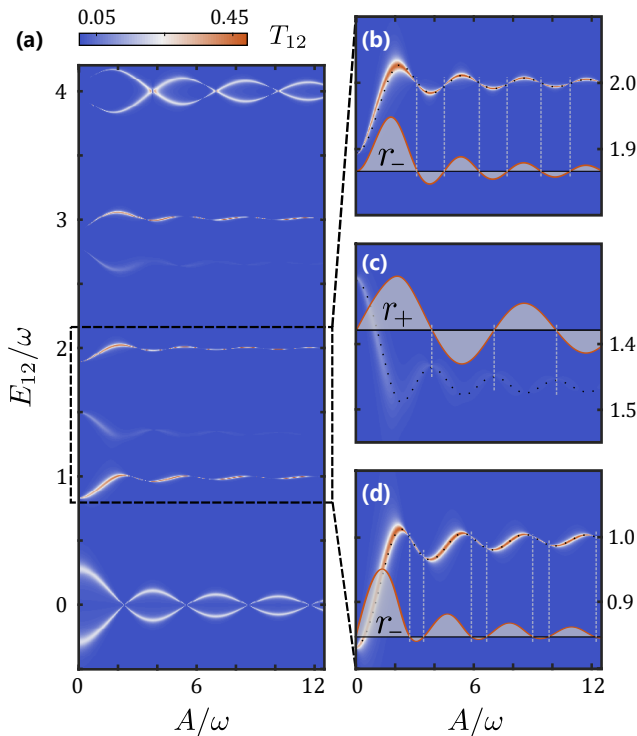


FIG. 2. **The transition amplitude of the driven three-level model.** (a) Time-averaged probability T_{12} as a function of driving amplitude A and energy spacing E_{12} with parameters $g_1 = 0.1$ GHz, $g_2 = 1$ GHz, $E_1 = -3E_2$ and $E_3 \equiv 0$. Significant transition is observed at the resonant condition of Eq. 6. The region of $E_{12}/\omega \in [0.8, 2.2]$ are zoomed in (b)-(d), in which the black dashed line represent the resonance indicated by H_{eff} , and the shaded functions are the effective couplings of r_{\pm} , roots of which yield the break points.

$g_2 = 1$ GHz and $\omega = 4$ GHz based on Floquet theorem (see Appendix. B 2) in Fig. 2 (a), focusing mainly on the long-term averaged transition rate T_{ij} between $|i\rangle$ and $|j\rangle$ captured by

$$T_{ij} = \lim_{t \rightarrow \infty} \frac{1}{t} \int_0^t P_{ij}(\tau) d\tau, \quad P_{ij}(\tau) = |\langle i|U(\tau)|j\rangle|^2. \quad (5)$$

Notice that T_{ij} in the next passage is calculated based on Floquet theorem while P_{ij} is based on numerical integration of Schrödinger equation or Lindblad master equation. Details in the black dashed box is enlarged in Fig. 2 (b)-(d), in which the analytical results from the above effective model are presented by black dots, exhibiting an excellent agreement with the simulation. The resonance transition happens at

$$E_{12} = \{n\omega + E_{32}, n\omega\} + \mathcal{O}(J_N^2/\omega), \quad (6)$$

for the two multifrequency resonances between $|1\rangle$ and $|2\rangle$, $|3\rangle$, respectively. This result suggests that, first, Rabi oscillation based on multifrequency resonance is possible (see Appendix C), and second, these two branches can be analogue to ATS, while the splitting is modulated in

the form of $J_N(A/\omega)$ as is shown in Fig. 2 (b)-(d) by the black dashed line, and is *almost* independent on the driving for strong drive $A/\omega \gg 1$.

These results exhibit two remarkable features. Firstly, we observe some break points, at which T_{12} is vanished. To evaluate the transition amplitude, we diagonalize the subspace of $\{|2\rangle, |3\rangle\}$ as $\text{diag}(E_+, E_-)$, yielding an effective coupling r_{\pm} between them, which are presented in the inset in Fig. 2 (b)-(d), showing the break points occur at $r_{\pm} = 0$ exactly. The break points means tunneling between $|1\rangle$ and $|2\rangle$ is forbidden in this condition. This is similar to the coherent destruction of tunneling in driven two-level systems [18, 22, 46], while extending to multilevel condition. Secondly, these points exhibit some striking odd-even alternative effect. Assuming $g_1 J_{N-n} \ll g_2 J_N$, for two branches of $E_{12} = n\omega$ and $E_{13} = 2n\omega$, the transition is determined by r_- and r_+ , respectively. Assuming that Δ' is ignorable, we investigate r_- in the condition of $E_{12} - n\omega = E_-$ and r_+ for $E_{12} - n\omega = E_+$ as follows

$$\begin{aligned} r_- &\propto \xi g_2 J_N - g_1 J_{N-n} \Delta, \\ r_+ &\propto \xi g_2 J_N + g_1 J_{N-n} (E_+ - \Delta). \end{aligned} \quad (7)$$

By substituting Δ , ξ in the condition of $E_{12} = n\omega$, we find $r_- \propto \sum_{m \neq N} g_1 g_2^2 (J_{m-n} J_m J_N - J_m^2 J_{N-n}) / (m\omega - E_{32})$ (see Appendix. C). According to the asymptotic behavior of Bessel function in the large A/ω limit, we find that for any even orders, $r_- \approx 0$, thus transition at $E_{12} = 2n\omega$ for large amplitude is forbidden, yielding the so-called odd-even effect. It is necessary to point out that this effect has been experimentally reported by Stehlik *et al.* [47], and then explained based on strong dissipation [28]. We show that it has a more intuitive interpretation without dissipation.

IV. CPT IN EFFECTIVE MODEL

Next, we focus on the various intriguing applications based on the effective model H_{eff} . The most straightforward application is CPT [4], in which the dark state is determined by the off-diagonal elements. When ξ is ignorable, we expect the dark state to be

$$|\psi\rangle \propto g_2 J_N |1\rangle - g_1 J_{N-n} |2\rangle, \quad (8)$$

where the minus sign reflects the cancellation of transition amplitude from these two states to the shuttle state $|3\rangle$. The dark state means that the transition between $|\psi\rangle$ and $|3\rangle$ is strictly forbidden, which is corresponds to suppression in current in experiments.

We demonstrate the CPT by the averaged transition amplitude $T_{\psi 3}$ from some initial state $|\psi(\theta)\rangle = \cos(\theta)|1\rangle + \sin(\theta)|2\rangle$ to $|3\rangle$ with $g_{1,2} = 1$ GHz. In the vicinity of $E_{12} = 2\omega$ and $E_{32} = \omega$, the effective couplings are given by $\tilde{g}_{1,2} = g_{1,2} J_{\pm 1}(A/\omega)$, and the dark state $|\psi\rangle$ is then defined by $|\phi(\pi/4)\rangle$. Numerical simulation of averaged transition amplitude $T_{\psi 3}$ is shown in Fig. 3 (a), in

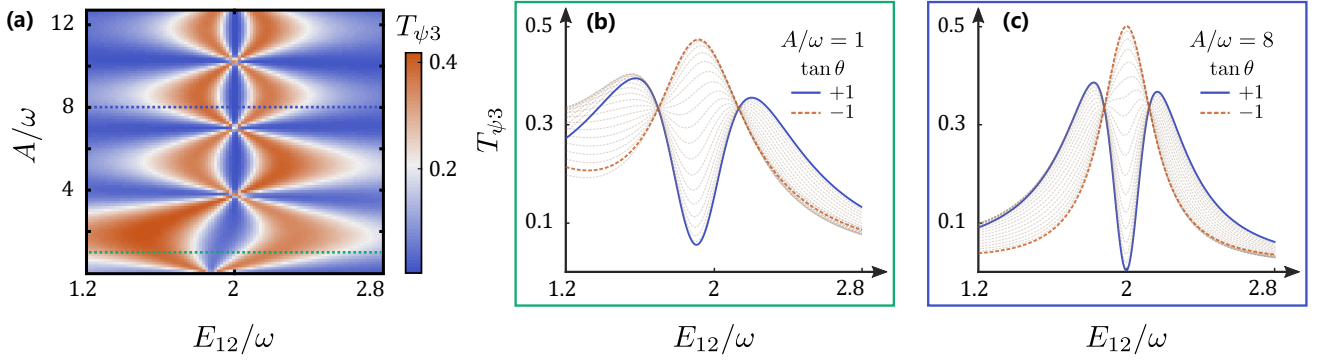


FIG. 3. **CPT based on the effective three-level model.** (a) Averaged transition amplitude $T_{\psi 3}$ as a function of E_{12} and A , with $E_{12} = 2E_{32}$, $g_1 = g_2 = 1$ GHz, $\omega = 4$ GHz and $\theta = \pi/4$. We focus on the region of $E_{12} \approx 2\omega$ with effective couplings given by $g_1 J_{-1}(A/\omega)$ and $g_2 J_1(A/\omega)$, respectively, from Eq. 4. As a result, $|\psi(\pi/4)\rangle$ is the dark state in case of $E_{12} = 2\omega$ with ignorable Δ , Δ' and ξ . (b) and (c) show the cross-sections at $A/\omega = 1$ and 8, respectively, with different initial state by scanning the relative phase in $|\psi(\theta)\rangle$. When A/ω is not large enough, the dip will not approach zero due to the tiny contribution of Δ , Δ' and ξ .

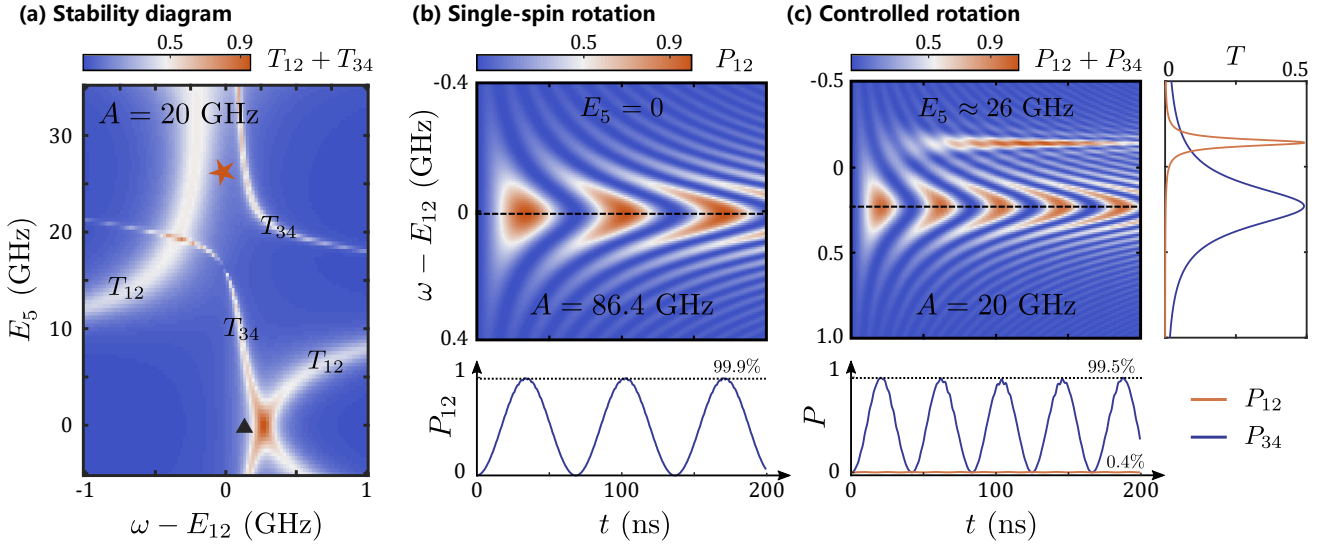


FIG. 4. **Quantum gate via Rabi oscillation in the ST system.** (a) Total transition amplitude $T_{12} + T_{34}$ vs detuning and shuttle energy, in which T_{12} and T_{34} response differently to detuning E_5 . Parameters used in simulation are $g_1 = 1$ GHz, $g_2 = 2$ GHz, $E_1 = -E_4 = 40$ GHz and $E_2 = -E_3 = 10$ GHz. (b) Single spin rotation by demonstrated Rabi chevron with $E_5 = 0$, $A = 86.4$ GHz. The on-resonance oscillation at resonance exhibit of maximal amplitude over 99.9%. (c) The two-qubit conditional-rotation gate with $E_5 = 26$ GHz and $A = 20$ GHz, in which P_{12} and P_{34} resonant at different frequencies. The maximal transition amplitude P_{12} is around 99.5%, with unexpected amplitude of P_{34} 0.4%.

which the suppression of transition amplitude is observed around $E_{12} = 2\omega$ for a wide range of A/ω . Two cross-sections with $A/\omega = 1.0$ and 8.0 are presented in Fig. 3 (b) and (c), respectively, from which we figure out that with the increasing of A/ω , the contribution of the off-diagonal coupling ξ becomes less important, and $|\psi(\pi/4)\rangle$ gets "darker". Moreover, the initial state is crucial to observe CPT since the only detectable state is the shuttle state. For the state orthogonal to $|\psi\rangle$ ($\tan(\theta) = -1$), a resonant peak appears as is shown in both Fig. 3 (b) and (c). Since the similar three-level models can also be obtained from the five-level model based on ST system, we expect that similar features including ATS, odd-even

effect and CPT to be observed in ST systems.

V. IMPROVEMENT IN QUANTUM GATES

A more attractive application is the possible improvement of quantum gates, which has the potential advantage of high fidelity and fast operation. In this proposal, the state leakage to shuttle state is suppressed by tuning of A/ω rather than large detuning, which is widely used in previous experiment [41, 42, 48]. According to H_{eff} in Eq. 4, leakage is determined by couplings to shuttle state, while the spin manipulation time is most relevant

to the synthetic coupling ξ . Larger detuning yields a higher order of Bessel function appeared in H_{eff} , which suppresses the leakage whereas fast operation is also hindered. However, tuning of A/ω enables the suppression of state leakage and maintains the fast operation simultaneously. That is to say, state manipulation can be implemented in the regime of small detuning, which additionally means a greater exchange coupling strength in ST system.

In Fig. 4 (a), we present the single spin rotation between $|\uparrow, \uparrow\rangle \leftrightarrow |\uparrow, \downarrow\rangle$ (T_{12}) and $|\downarrow, \downarrow\rangle \leftrightarrow |\downarrow, \uparrow\rangle$ (T_{34}) versus frequency and detuning energy E_5 . At the solid triangle point with zero detuning, these two transitions are degenerate, which means that the rotation of spins are independent on each other and single-spin rotation can be constructed. Otherwise, transitions occur at different driving frequency, indicating that rotation of spin on the right is dependent on the left spin, which can be referred to as controlled rotation. Fig. 4 (b) exhibits the single-spin rotation simulated with parameters $g_1 = 1$ GHz, $g_2 = 2$ GHz and amplitude of 86.4 GHz. The cross-section of the chevron at resonance exhibits high-fidelity exceeding 99.9% with fast manipulation time of 35 ns. Moreover, the working point of $E_5 = 0$ is a symmetric operation point, which is robust to charge noise in E_5 [49].

When $E_5 \neq 0$, the two transitions shift differently as shown in Fig. 4 (a), and controlled rotation can be constructed. In Fig. 4 (c), we present the controlled rotation with $E_5 \approx 26$ GHz as indicated by the red pentagram in Fig. 4 (a) and set $A = 20$ GHz. The result manifests as two overlapped chevrons — one is narrow peaked at $\omega - E_{12} \approx -0.2$ GHz and one is broad peaked at $\omega - E_{12} \approx 0.2$ GHz, standing for T_{34} and T_{12} , respectively. The cross-section indicated by black dashed line in Fig. 4 exhibits a resonant transition with an amplitude over 99.5% and a suppressed off-resonant rotation amplitude of 0.4%. The frequency difference between two resonant peaks indicates a significant exchange coupling strength, which is essentially induced by small detuning.

VI. COHERENT STATE TRANSFER VIA ADIABATIC PASSAGE

The above quantum gate can also be realized based on the scheme of adiabatic passage, which has been demonstrated in various platforms [11–13] besides QDs system. Here, we need to adiabatically modulate the effective $H_{\text{eff}}(t)$, assuming that the modulating frequency is much smaller than the driving frequency. Comparing to the former works where the off-diagonal terms are tuned independently, g_i are assumed to be uncontrollable constants in our model, leaving only the relevant controlling parameter to be the slow-varying amplitude $A(t)$. We accomplish this process by

$$A(t) = 100 \sin^2(\pi t/2t_f), \quad 0 \leq t \leq t_f, \quad (9)$$

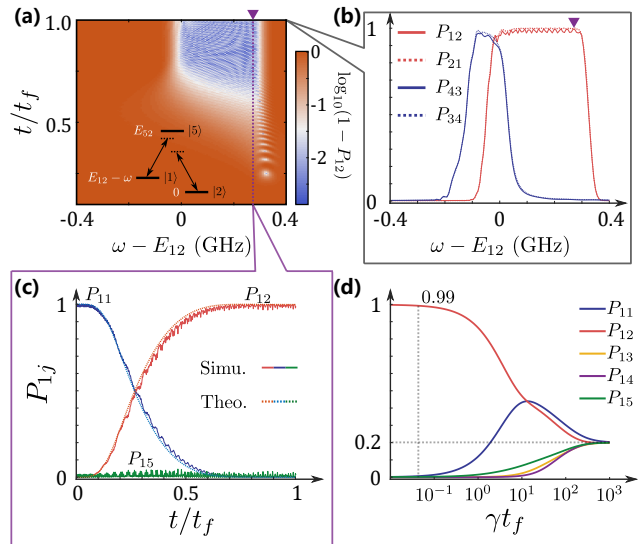


FIG. 5. **Quantum gate via adiabatic passage in the ST system.** (a) Infidelity $\log_{10}(1 - P_{12}(t))$ with respect to detuning $\omega - E_{12}$ for $t \leq t_f$. Inset shows the effective three-level model by $|1\rangle$, $|2\rangle$ and $|5\rangle$. (b) The final probability $P_{ij}(t_f)$ as a function of $\omega - E_{12}$, in which the triangle point can be used for controlled-rotation gate. (c) The cross-section along the dashed line in (a), from both fully simulation of the time-dependent Hamiltonian (solid curves) and that by the effective Hamiltonian H_{eff} (dashed curves). (d) Probability with Lindblad dissipation of the same behavior of (c), with dissipation strength γ . For $t_f < T_2/10$, transition amplitude $P_{12} > 99\%$; and for $t_f = T_2/20$ and in the long-time limit, state thermalization is reached with $P_{1i} = 1/5$ when $t_f > 10^2 T_2$.

where $t_f = 1 \mu\text{s}$ is the total evolution time. Noticed that this is not the most optimum solution of this process, which we leave for experimental exploration in the future. In the effective Hamiltonian, all the correlations such as ξ , Δ and Δ' are included in the sense that when $A(t)$ is small, they may be important. We investigate the adiabatic process in five-level ST system by $i\partial_t|\psi\rangle = H(t)|\psi\rangle$ with different driving frequencies. With the modulation on driving amplitude, state transfer occurs in a wide range of driving frequency as shown in Fig. 5 (a), where the color represents the logarithmic result of infidelity $1 - P_{12}(t)$. This model is equivalent to a three-level Λ configuration composed of $|1\rangle$, $|2\rangle$ and $|5\rangle$, while the effective couplings are only tuned by driving amplitude. In Fig. 5 (b) we present different probability $P_{ij}(t_f)$ with the same adiabatic passage as a function of driving frequency. Based on the fact that transitions are addressable via driving frequency, controlled rotation can be constructed. e.g., when $\omega - E_{12} = 0.27$ GHz as is label by the solid purple triangle in both Fig. 5 (a) and (b), P_{12} and P_{21} are significant while P_{34} P_{43} are subtle. In addition, the plateau of $P_{ij}(t_f)$ indicates that the gate is robust to frequency/energy spacing shift.

We next validate the approximation of $H_{\text{eff}}(t)$. In Fig. 5 (c), we compare the full simulation and the result from

$H_{\text{eff}}(t)$ along the dashed vertical line in Fig. 5 (a). These curves are in good agreement, especially in the regime of $A(t) \rightarrow A(t_f)$. In Appendix. B 3, we show that H_{eff} in Eq. 4 can be more efficient than that from Magnus expansion [45]. We also investigate the influence from dissipation described by the following Lindblad master equation

$$\dot{\rho} = -i[H(t), \rho] + \sum_{k \neq 0} \left[L_k \rho L_k^\dagger - \frac{1}{2} \{L_k^\dagger L_k, \rho\} \right], \quad (10)$$

where the summation represents the non-unitary evolution and $L_k = \sqrt{\nu_k}|k\rangle\langle k|$, for $k = 1, \dots, 5$, account for the white-noise fluctuations on each level. Notice that we neglect the contribution of energy relaxation between these levels for the reason that in QDs, $T_1 \gg T_2$. We plot $P_{1j}(t_f)$ as a function of γ (assuming $\nu_k = \gamma = 1/T_2$), showing a transition from the perfect gate operation with $P_{12}(t_f) \rightarrow 1$ to $P_{1j} = 1/5$ as the maximal mixed state, which can be reached when $t_f > 10^2 T_2$. Moreover, when $t_f = T_2/20$, the fidelity $P_{12}(t_f)$ can exceed 0.99.

VII. CONCLUSION

To conclude, we study the LZS process in two specific multilevel systems in QDs, and proposes an effective model, which provides some insights into the process. Based on the effective model, we demonstrate the ATS and CPT induced by longitudinal drive, and figure out the so-called odd-even effect in an intuitive way. In addition, from the effective model we propose that state manipulation in similar systems can be implemented in small detuning regime, since the large detuning is not necessary but poses a limitation to operation time. Besides, the system is robust to charge noise on detuning when detuning is zero. Moreover, noise insensitive qubit manipulation can be realized by adiabatic passage according to the effective model. Some more intriguing application of our scheme can be realized by carefully controlling of the driving fields in the concrete physical systems. From our scheme, the coupling strengths are modulated via the longitudinal driving field, thus has broad application in the QDs for their applications in analogue quantum simulation and quantum simulation.

VIII. ACKNOWLEDGMENTS

This work was supported by the National Key Research and Development Program of China (Grant No.2016YFA0301700), the National Natural Science Foundation of China (Grants No. 12074368, 12034018, 11625419 and 61922074), X. H. acknowledges financial support by U.S. ARO through No. W911NF1710257.

Appendix A: Energy levels in QDs and the associated parameters

Qubits in QDs have the advantages of electric controlling, potential integratable, fast gate operation, and high working temperature. The levels for the hybrid system in Fig. 1 (a) is composed by one level at the left dot and two levels at the right dot. For three electrons, its total spin is decoupled into one quadruplet with $S = 3/2$ and two doublets with $S = 1/2$, for $-S \leq s_z \leq S$, in which the spin independent potential only mixes states of the same S and s_z . Following Refs. [32, 36], we define the qubits using the three states with $s_z = 1/2$. A full theoretical analysis including all possible interactions can be found in Ref. 34. It has been realized in several experiments based on QDs, with typical parameters of $g_1 \sim g_2 \sim \mathcal{O}(1)$ GHz (see Table I), which are determined by the barrier tunneling. We use these parameters for the searching of ATS and odd-even effect in Fig. 2.

The physics in the ST system is a bit different. For two electrons in the two dots, the lowest four qubit states are given in Eq. 2, where the shuttle state $|5\rangle$ means two electrons at the left dot, forming a singlet state. Here the transition from $|1\rangle$ and $|4\rangle$ to $|5\rangle$ involves the spin flip during tunneling (due to spin-orbit coupling), which is weak in silicon ($g_1 \sim 20$ MHz in Table I). It can be greatly enhanced in semiconductors with strong spin-orbit coupling. The coupling by g_2 is induced by tunneling, which can in principle be comparable to that in the hybrid qubit system for the reason of the same mechanism. We summarize the parameters in these QDs in Table I and use these parameters for demonstration of CPT in Fig. 3 and quantum gates in Fig. 4 and Fig. 5.

TABLE I. Summarized experimental parameters in the unit of GHz for the hybrid system and ST system. In the ST system, g_{2n} is not specified for its wide range of tunability in experiments by the inter-dot barrier from MHz to tens of gigahertz.

	Hybrid		ST	
	$g_1/h, g_2/h$	E_{12}/h	g_1/h	E_{12}/h
Si/SiO ₂	-	-	0.021	0.032 [50]
Si/SiGe	2.6, 7.5	12 [33]	0.023 [51]	0.42 ^a
Ge/SiGe	-	-	-	0.56B ^b [41]
GaAs	4.6, 3.8	2.5 ~ 3.5 [35]	0.015	0.014 [37, 53]
NW (InAs)	-	-	0.44 ~ 14 [54]	4.2B
NW (InSb)	-	-	0.60	28B [55]
NW (Ge/Si)	-	-	4.8 ~ 15 [56]	0

^a Estimated by $g\mu_B\Delta B_x$ with $\Delta B_x = 15$ mT [52].

^b Proportional to external magnetic field B .

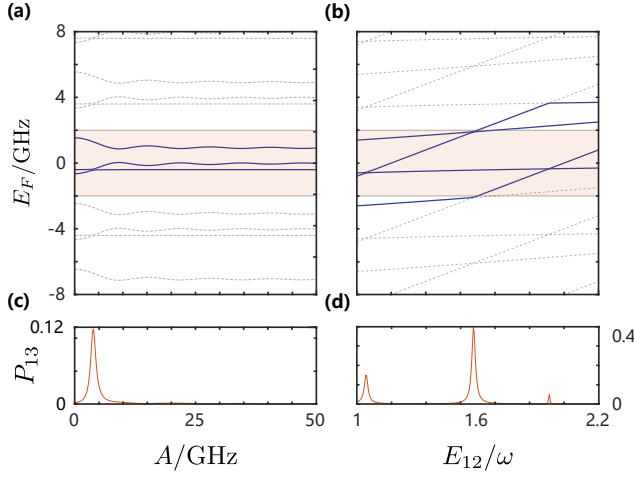


FIG. 6. **Floquet energy levels E_F and transition amplitude T_{13} versus A in (a) and E_{12} in (b), respectively.** The energy levels are presented in solid blue or dashed gray lines, while red shading area indicates the first Brillouin zone. The energy structure manifest a periodicity as Floquet theorem indicated. When energy level crossovers with each other, state transfer occurs, thus population in $|3\rangle$ can be detected as indicated by solid red lines in (c) and (d).

Appendix B: Derivation of effective Hamiltonian

1. Rotating frame for diagonal modulated system

We are dealing with a periodic system with strong diagonal modulating ($A \gg \omega$), which can not be directly explored using Floquet theorem for the searching of H_F . To this, a proper rotation of H by

$$U = \text{diag}(e^{i(E_2+n\omega)t}, e^{iE_2t}, e^{i(E_2+N\omega)t - i\frac{A \sin(t\omega)}{\omega}}), \quad (\text{B1})$$

can be applied, and accordingly

$$\tilde{H}(t) = \begin{pmatrix} E_{12} - n\omega & c(t)g_1 e^{in\omega t} \\ 0 & c(t)g_2 \\ c^*(t)g_1 e^{-in\omega t} & c^*(t)g_2 & E_{32} - N\omega \end{pmatrix}, \quad (\text{B2})$$

with $E_{ij} = E_i - E_j$ and $c(t) = e^{\frac{iA \sin(\omega t)}{\omega} - iN\omega t} = \sum_{\nu} J_{\nu}(A/\omega) e^{i(\nu - N)\omega t}$. By proper, we mean that (i) the diagonal matrix elements should be restricted to the first Brillouin zone; and (ii) the new Hamiltonian $\tilde{H}(t)$ should have the same periodicity as $H(t)$; and (iii) the degrees of freedom in U should be uniquely determined.

2. Floquet-Schrödinger equation and numerical simulation

The Floquet theorem provides a general framework to study the linear models with periodic modulation in the time domain. For $i\partial_t|\psi\rangle = H(t)|\psi\rangle$, where $H(t)$ was defined above, we can write $|\psi\rangle = e^{-iqt}|u(t)\rangle$, where q

is the quasi-energy and $|u(t)\rangle$ is a periodic function with period T . In this way, we have

$$(H(t) - i\partial_t)|u(t)\rangle = q|u(t)\rangle, \quad |u(t)\rangle = |u(t+T)\rangle. \quad (\text{B3})$$

This equation can be cast to a stationary equation, assuming that $|u(t)\rangle = \sum_{n,\alpha} c_{n\alpha}|n,\alpha\rangle$, where $|n,\alpha\rangle = |\alpha\rangle e^{in\omega t}$. If one assume $|\mathcal{U}\rangle$ the proper order of $c_{n\alpha}$ for $n \in \mathbb{Z}$, we find the Floquet-Schrödinger equation as $\mathcal{H}_F|\mathcal{U}\rangle = q|\mathcal{U}\rangle$ [43], with matrix elements as

$$\langle \alpha, n | \mathcal{H}_F | \beta, m \rangle = H_{\alpha\beta}^{(n-m)} + n\omega \delta_{nm} \delta_{\alpha\beta}, \quad (\text{B4})$$

with $H_{\alpha\beta}^{(n-m)}$ the $(n-m)$ th Fourier coefficient of matrix element $H_{\alpha\beta}$. Though \mathcal{H}_F is a matrix of infinity size, in numerical simulation, we can make a finite truncation of n ($|n| \leq N_c = 20$) to calculate the quasienergy q , which is shown in Fig. 6 (a)-(b). Obviously, the spectrum is a repeating of levels in the first Brillouin zone shifted by ω . We will focus on the first Brillouin zone defined as $\mathcal{B} = [-\omega/2, \omega/2]$.

Based on \mathcal{H}_F , we can evaluate the transition amplitude from $|\beta\rangle$ to $|\alpha\rangle$ by

$$U_{\alpha,\beta}(t; t_0) = \sum_n \langle \alpha, n | e^{-i\mathcal{H}_F(t-t_0)} | \beta, 0 \rangle e^{in\omega t}, \quad (\text{B5})$$

where the summation collects the contributions from all orders of Fourier components. The averaged transition amplitude is then given by

$$T_{\alpha\beta}(t; t_0) = \sum_{m,n,\phi} \langle \alpha, n | \phi \rangle \langle \phi | \beta, 0 \rangle \langle \beta, m | \phi \rangle \langle \phi | \alpha, n \rangle e^{im\omega t_0}, \quad (\text{B6})$$

with $|\phi\rangle$ the eigenstates of \mathcal{H}_F . Our numerical results for this transition amplitude are shown in Fig. 6 (c) and (d), where the resonance transition are expected to happen at the degenerate points.

3. Effective Hamiltonian

We mainly present our results based on an effective Hamiltonian H_{eff} by eliminating the off-diagonal couplings between different zones in \mathcal{H}_F , which take the form of $g_i J_{\nu}$, decaying with the increasing of ν . This is achieved by a unitary transformation of $\mathcal{H}_F = U^\dagger \mathcal{H}_F U$, where $U = e^{-S}$. Based on the procedure in Ref. [44], we define S as

$$\mathcal{E}_{ml} S_{ml} = \sum_{m'} \frac{(\mathcal{H}_F)_{mm'} (\mathcal{H}_F)_{m'l}}{\mathcal{E}_{m'l}} - \sum_{l'} \frac{(\mathcal{H}_F)_{ml'} (\mathcal{H}_F)_{l'l}}{\mathcal{E}_{m'l}}, \quad (\text{B7})$$

where here m and l includes the index of n and α in Eq. B4 and $\mathcal{E}_{ml} = (\mathcal{H}_F)_{mm} - (\mathcal{H}_F)_{ll}$ for short. The basis is also changed accordingly as $|\tilde{i}\rangle = e^{-S}|i\rangle$. In this way, equivalent effective Hamiltonian used in the main text

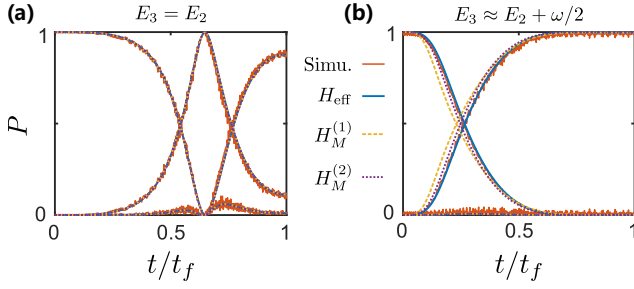


FIG. 7. **Comparison of two effective Hamiltonians.** State transfer via adiabatic passage is investigated in different regime. (a) For $E_3 = E_2$, H_{eff} is equivalent to $H_M^{(1)}$, and all these effective models approximate the simulation result well. (b) For $E_3 \approx E_2 + \omega/2$, effective levels are close to the Brillouin zone boundary, $H_M^{(1,2)}$ deviate from the simulation while H_{eff} is still accurate.

is obtained, in which Δ', Δ, ξ are corrections induced by the influence from other blocks, with

$$\Delta' = \sum_{m \neq N-n} \frac{(g_1 J_m)^2}{E_{13} + m\omega}, \quad \Delta = \sum_{m \neq N} \frac{(g_2 J_m)^2}{E_{23} + m\omega}, \quad (\text{B8})$$

$$\xi = \sum_{m \neq N} \frac{g_1 g_2 J_m J_{m-n}}{2(E_{23} + m\omega)} + \sum_{m \neq N-n} \frac{g_1 g_2 J_m J_{m+n}}{2(E_{13} + m\omega)}. \quad (\text{B9})$$

The effective model may also be computed using the Magnus expansion [45]. Following the same rotation, we can write $H(t) = H_0 + \sum_{n \neq 0} H_n e^{in\omega t}$, and we have

$$H_M = H_0 + \sum_{n>0} \frac{[H_n, H_{-n}]}{n\omega} + \dots \quad (\text{B10})$$

Comparing to the effective model by Magnus expansion, our result is more effective in a broader regime. For clarity, we denote the result derived by Magnus expansion as $H_M^{(1)}$, $H_M^{(2)}$ for first- and second-order result, respectively. The adiabatic state transfer given by $H_M^{(1)}$, $H_M^{(2)}$, H_{eff} and numerical simulation is presented in Fig. 7, in which two conditions are compared, namely, when energy levels far from and close to Brillouin boundary, exhibited in (a), (b) respectively. From the comparison, we notice that H_{eff} is effective for both cases while $H_M^{(1,2)}$ deviates from the numerical result. Similar comparison is carried out in many other conditions and yields the same difference, indicating that H_{eff} is more effective for the driven system studied in the main text.

Appendix C: ATS and odd-even effect

To address the resonant transition presented in the main text, we diagonalize the subspace of $\{|2\rangle, |3\rangle\}$. Ef-

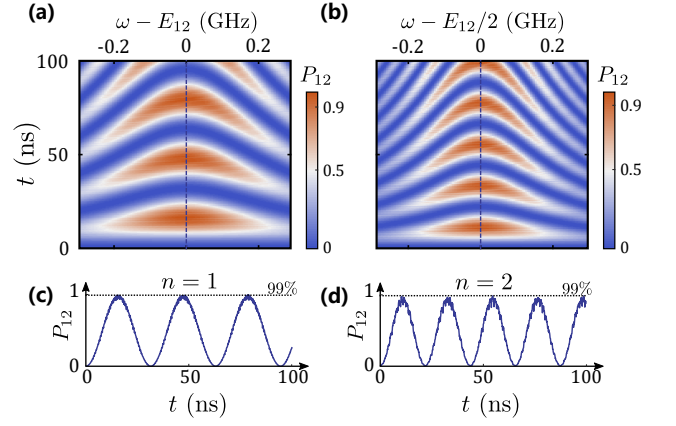


FIG. 8. **Multifrequency qubit manipulation.** Rabi oscillation chevrons for $n = 1$ (a) and $n = 2$ (b), resonant oscillation amplitude of which is presented in (c) and (d) respectively.

fective Hamiltonian is then given by

$$H_{\text{eff}} = \begin{pmatrix} E_{12} - n\omega & r_+ & r_- \\ r_+^* & E_+ & 0 \\ r_-^* & 0 & E_- \end{pmatrix}, \quad (\text{C1})$$

with E_{\pm} the eigenenergies of subspace spanned by $\{|2\rangle, |3\rangle\}$ and r_{\pm} the corresponding coupling strength. For weak couplings, the transition is determined by $E_{12} - n\omega = E_{\pm}$, resulting in the ATS induced by longitudinal drive as mentioned in the main text. Notice that the resonant condition indicates state manipulation based on multifrequency. To demonstrate that, we present a numerical simulation result in Fig. 8 (a), (b), where we present Rabi oscillation for $E_{12} = \omega$ and $E_{12} = 2\omega$.

Analogue to coherent destruction of tunneling in TLS, intervals are found when the relevant effective coupling term meets its zero points, and interestingly, the Bessel functions induces a parity-dependent result, which is referred to as odd-even effect in the main text. According to H_{eff} , the resonance is described by $E_{12} - n\omega = E_{\pm}$. One of the branch, namely, $E_{12} - n\omega = E_- \approx 0$, manifests the parity effect. e.g., for $E_{12} = n\omega$, we have

$$\begin{aligned} r_- &\propto \xi g_2 J_N - g_1 J_{N-n} \Delta \\ &= \sum_{m \neq N} \frac{g_1 g_2^2}{m\omega - E_{23}} (J_{m-n} J_m J_N - J_m^2 J_{N-n}), \end{aligned} \quad (\text{C2})$$

on the other hand, for the other branch $E_{12} - n\omega = E_+$, in the vicinity of $E_{13} = (N-n)\omega$, we have r_+ proportional to

$$\begin{aligned} &\sum_{m \neq N} \frac{g_1 g_2^2 J_m J_{m-n} J_N}{2(E_{23} + m\omega)} + \sum_{m \neq N-n} \frac{g_1 g_2^2 J_m J_{m+n} J_N}{2(m+n-N)\omega} \\ &+ g_1 J_N \left(E_{32} - N\omega - \sum_{m \neq N} \frac{(g_2 J_m)^2}{E_{23} + N\omega} \right) \end{aligned} \quad (\text{C3})$$

For Bessel functions of the first kind, we know the asymptotic behavior of

$$J_n(x) \approx \sqrt{\frac{2}{\pi x}} \cos[x - (2n + 1)\pi/4], \quad x \gg n. \quad (\text{C4})$$

This property guarantees $r_- \approx 0$ at $E_{12} = n\omega$ for even ns when $A/\omega \gg N - n$, $m - n$, while odd ns , break points can be found around $E_{12} = n\omega$ when

$J_{m-n}J_N = J_mJ_{N-n}$, but this condition could not always be fulfilled. For the other branch of ATS, odd-even effect does not. However, odd-even effect would disappear when $E_3 > A$, in other words, when system does not go through anti-crossings, which is in accordance with experiment [47]. It can be interpreted with the relation $N \approx E_{23}/\omega > A/\omega$, which means $E_3 > A$ undermines the approximation condition $A/\omega \gg N - n$ for small n .

-
- [1] S. H. Autler and C. H. Townes, Stark effect in rapidly varying fields, *Phys. Rev.* **100**, 703 (1955).
- [2] X. Xu, B. Sun, P. R. Berman, D. G. Steel, A. S. Bracker, D. Gammon, and L. J. Sham, Coherent Optical Spectroscopy of a Strongly Driven Quantum Dot, *Science* **317**, 929 (2007).
- [3] M. A. Sillanpää, J. Li, K. Cicak, F. Altomare, J. I. Park, R. W. Simmonds, G. S. Paraoanu, and P. J. Hakonen, Autler-Townes Effect in a Superconducting Three-Level System, *Phys. Rev. Lett.* **103**, 193601 (2009).
- [4] H. R. Gray, R. M. Whitley, and C. R. Stroud, Coherent trapping of atomic populations, *Opt. Lett.* **3**, 218 (1978).
- [5] C. Wei and N. B. Manson, Observation of the dynamic Stark effect on electromagnetically induced transparency, *Phys. Rev. A* **60**, 2540 (1999).
- [6] M. Bajcsy, A. S. Zibrov, and M. D. Lukin, Stationary pulses of light in an atomic medium, *Nature* **426**, 638 (2003).
- [7] M. D. Eisaman, A. André, F. Massou, M. Fleischhauer, A. S. Zibrov, and M. D. Lukin, Electromagnetically induced transparency with tunable single-photon pulses, *Nature* **438**, 837 (2005).
- [8] X. Xu, B. Sun, P. R. Berman, D. G. Steel, A. S. Bracker, D. Gammon, and L. J. Sham, Coherent population trapping of an electron spin in a single negatively charged quantum dot, *Nat. Phys.* **4**, 692 (2008).
- [9] M. Mücke, E. Figueroa, J. Bochmann, C. Hahn, K. Murr, S. Ritter, C. J. Villas-Boas, and G. Rempe, Electromagnetically induced transparency with single atoms in a cavity, *Nature* **465**, 755 (2010).
- [10] R. Röhlsberger, H. C. Wille, K. Schlage, and B. Sahoo, Electromagnetically induced transparency with resonant nuclei in a cavity, *Nature* **482**, 199 (2012).
- [11] T. Takekoshi, L. Reichsöllner, A. Schindewolf, J. M. Hutson, C. R. Le Sueur, O. Dulieu, F. Ferlaino, R. Grimm, and H.-C. Nägerl, Ultracold dense samples of dipolar rbc molecules in the rovibrational and hyperfine ground state, *Phys. Rev. Lett.* **113**, 205301 (2014).
- [12] P. K. Molony, P. D. Gregory, Z. Ji, B. Lu, M. P. Köppinger, C. R. Le Sueur, C. L. Blackley, J. M. Hutson, and S. L. Cornish, Creation of ultracold $^{87}\text{Rb}^{133}\text{Cs}$ molecules in the rovibrational ground state, *Phys. Rev. Lett.* **113**, 255301 (2014).
- [13] K. S. Kumar, A. Vepsäläinen, S. Danilin, and G. S. Paraoanu, Stimulated Raman adiabatic passage in a three-level superconducting circuit, *Nat. Commun.* **7**, 10628 (2016).
- [14] N. V. Vitanov, A. A. Rangelov, B. W. Shore, and K. Bergmann, Stimulated Raman adiabatic passage in physics, chemistry, and beyond, *Rev. Mod. Phys.* **89**, 015006 (2017).
- [15] M. O. Scully and M. S. Zubairy, *Quantum Optics* (Cambridge University Press, 1997).
- [16] S. Shevchenko, S. Ashhab, and F. Nori, Landau-Zener-Stückelberg interferometry, *Phys. Rep.* **492**, 1 (2010).
- [17] M. P. Silveri, J. A. Tuorila, E. V. Thuneberg, and G. S. Paraoanu, Quantum systems under frequency modulation, *Reports Prog. Phys.* **80**, 056002 (2017).
- [18] W. D. Oliver, Mach-Zehnder Interferometry in a Strongly Driven Superconducting Qubit, *Science* **310**, 1653 (2005).
- [19] D. M. Berns, M. S. Rudner, S. O. Valenzuela, K. K. Berggren, W. D. Oliver, L. S. Levitov, and T. P. Orlando, Amplitude spectroscopy of a solid-state artificial atom, *Nature* **455**, 51 (2008).
- [20] W. D. Oliver and S. O. Valenzuela, Large-amplitude driving of a superconducting artificial atom, *Quantum Inf. Process.* **8**, 261 (2009).
- [21] G. Cao, H.-O. Li, T. Tu, L. Wang, C. Zhou, M. Xiao, G.-P. G. C. G. P. G.-C. Guo, H.-W. W. Jiang, and G.-P. G. C. G. P. G.-C. Guo, Ultrafast universal quantum control of a quantum-dot charge qubit using Landau-Zener-Stückelberg interference, *Nat. Commun.* **4**, 1401 (2013).
- [22] J. Stehlik, Y. Dovzhenko, J. R. Petta, J. R. Johansson, F. Nori, H. Lu, and A. C. Gossard, Landau-Zener-Stückelberg interferometry of a single electron charge qubit, *Phys. Rev. B* **86**, 121303 (2012).
- [23] F. Forster, G. Petersen, S. Manus, P. Hänggi, D. Schuh, W. Wegscheider, S. Kohler, and S. Ludwig, Characterization of qubit dephasing by Landau-Zener-Stückelberg-Majorana interferometry, *Phys. Rev. Lett.* **112**, 116803 (2014).
- [24] P. Huang, J. Zhou, F. Fang, X. Kong, X. Xu, C. Ju, and J. Du, Landau-Zener-Stückelberg interferometry of a single electron spin in a noisy environment, *Phys. Rev. X* **1**, 1 (2011).
- [25] X. Mi, S. Kohler, and J. R. Petta, Landau-Zener interferometry of valley-orbit states in Si/SiGe double quantum dots, *Phys. Rev. B* **98**, 161404 (2018).
- [26] S. N. Shevchenko, A. I. Ryzhov, and F. Nori, Low-frequency spectroscopy for quantum multilevel systems, *Phys. Rev. B* **98**, 195434 (2018).
- [27] A. Bogan, S. Studenikin, M. Korkusinski, L. Gaudreau, P. Zawadzki, A. S. Sachrajda, L. Tracy, J. Reno, and T. Hargett, Landau-Zener-Stückelberg-Majorana Interferometry of a Single Hole, *Phys. Rev. Lett.* **120**, 207701 (2018).
- [28] J. Danon and M. S. Rudner, Multilevel interference resonances in strongly driven three-level systems, *Phys. Rev.*

- Lett.* **113**, 247002 (2014).
- [29] X. Zhang, H.-O. Li, G. Cao, M. Xiao, G.-C. Guo, and G.-P. Guo, Semiconductor quantum computation, *Nat. Sci. Rev.* **6**, 32 (2019).
- [30] L. Petit, H. G. J. Eenink, M. Russ, W. I. L. Lawrie, N. W. Hendrickx, S. G. J. Philips, J. S. Clarke, L. M. K. Vandersypen, and M. Veldhorst, Universal quantum logic in hot silicon qubits, *Nature* **580**, 355 (2020).
- [31] C. H. Yang, R. C. C. Leon, J. C. C. Hwang, A. Saraiva, T. Tantt, W. Huang, J. Camirand Lemyre, K. W. Chan, K. Y. Tan, F. E. Hudson, K. M. Itoh, A. Morello, M. Pioro-Ladrière, A. Laucht, and A. S. Dzurak, Operation of a silicon quantum processor unit cell above one kelvin, *Nature* **580**, 350 (2020).
- [32] Z. Shi, C. B. Simmons, J. R. Prance, J. K. Gamble, T. S. Koh, Y.-P. Shim, X. Hu, D. E. Savage, M. G. Lagally, M. A. Eriksson, M. Friesen, and S. N. Coppersmith, Fast Hybrid Silicon Double-Quantum-Dot Qubit, *Phys. Rev. Lett.* **108**, 140503 (2012).
- [33] D. Kim, Z. Shi, C. B. Simmons, D. R. Ward, J. R. Prance, T. S. Koh, J. K. Gamble, D. E. Savage, M. G. Lagally, M. Friesen, S. N. Coppersmith, and M. A. Eriksson, Quantum control and process tomography of a semiconductor quantum dot hybrid qubit, *Nature* **511**, 70 (2014).
- [34] Z. Shi, C. B. Simmons, D. R. Ward, J. R. Prance, X. Wu, T. S. Koh, J. K. Gamble, D. E. Savage, M. G. Lagally, M. Friesen, S. N. Coppersmith, and M. A. Eriksson, Fast coherent manipulation of three-electron states in a double quantum dot, *Nat. Commun.* **5**, 1 (2014).
- [35] G. Cao, H.-O. Li, G.-D. Yu, B.-C. Wang, B.-B. Chen, X.-X. Song, M. Xiao, G.-C. G.-P. Guo, H.-W. Jiang, X. Hu, and G.-C. G.-P. Guo, Tunable Hybrid Qubit in a GaAs Double Quantum Dot, *Phys. Rev. Lett.* **116**, 086801 (2016).
- [36] D. P. DiVincenzo, D. Bacon, J. Kempe, G. Burkard, and K. B. Whaley, Universal Quantum Computation with the Exchange Interaction, *Nature* **408**, 339 (2000).
- [37] J. R. Petta, A. C. Johnson, J. M. Taylor, E. A. Laird, A. Yacoby, M. D. Lukin, C. M. Marcus, M. P. Hanson, and A. C. Gossard, Coherent Manipulation of Coupled Electron Spins in Semiconductor Quantum Dots, *Science* **309**, 2180 (2005).
- [38] M. Pioro-Ladrière, T. Obata, Y. Tokura, Y. S. Shin, T. Kubo, K. Yoshida, T. Taniyama, and S. Tarucha, Electrically driven single-electron spin resonance in a slanting Zeeman field, *Nat. Phys.* **4**, 776 (2008).
- [39] S. Foletti, H. Bluhm, D. Mahalu, V. Umansky, and A. Yacoby, Universal quantum control of two-electron spin quantum bits using dynamic nuclear polarization, *Nat. Phys.* **5**, 903 (2009).
- [40] W. Huang, C. H. Yang, K. W. Chan, T. Tantt, B. Hensen, R. C. Leon, M. A. Fogarty, J. C. Hwang, F. E. Hudson, K. M. Itoh, A. Morello, A. Laucht, and A. S. Dzurak, Fidelity benchmarks for two-qubit gates in silicon, *Nature* **569**, 532 (2019).
- [41] N. W. Hendrickx, D. P. Franke, A. Sammak, G. Scappucci, and M. Veldhorst, Fast two-qubit logic with holes in germanium, *Nature* **577**, 487 (2020).
- [42] K. Takeda, A. Noiri, J. Yoneda, T. Nakajima, and S. Tarucha, Resonantly Driven Singlet-Triplet Spin Qubit in Silicon, *Phys. Rev. Lett.* **124**, 117701 (2020).
- [43] J. H. Shirley, Solution of the Schrödinger Equation with a Hamiltonian Periodic in Time, *Phys. Rev.* **138**, B979 (1965).
- [44] R. Winkler, *New York*, Springer Tracts in Modern Physics, Vol. 191 (Springer Berlin Heidelberg, Berlin, Heidelberg, 2003) p. 228.
- [45] N. Goldman and J. Dalibard, Periodically Driven Quantum Systems: Effective Hamiltonians and Engineered Gauge Fields, *Phys. Rev. X* **4**, 031027 (2014).
- [46] S. Ashhab, J. R. Johansson, A. M. Zagoskin, and F. Nori, Two-level systems driven by large-amplitude fields, *Phys. Rev. A* **75**, 063414 (2007).
- [47] J. Stehlik, M. D. Schroer, M. Z. Maijale, M. H. Degani, and J. R. Petta, Extreme Harmonic Generation in Electrically Driven Spin Resonance, *Phys. Rev. Lett.* **112**, 227601 (2014).
- [48] D. M. Zajac, A. J. Sigillito, M. Russ, F. Borjans, J. M. Taylor, G. Burkard, and J. R. Petta, Resonantly driven CNOT gate for electron spins, *Science* **359**, 439 (2018).
- [49] F. Martins, F. K. Malinowski, P. D. Nissen, E. Barnes, S. Fallahi, G. C. Gardner, M. J. Manfra, C. M. Marcus, and F. Kuemmeth, Noise Suppression Using Symmetric Exchange Gates in Spin Qubits, *Phys. Rev. Lett.* **116**, 116801 (2016).
- [50] P. Harvey-Collard, N. T. Jacobson, C. Bureau-Oxton, R. M. Jock, V. Srinivasa, A. M. Mounce, D. R. Ward, J. M. Anderson, R. P. Manginell, J. R. Wendt, T. Pluym, M. P. Lilly, D. R. Luhman, M. Pioro-Ladrière, and M. S. Carroll, Spin-orbit Interactions for Singlet-Triplet Qubits in Silicon, *Phys. Rev. Lett.* **122**, 217702 (2019).
- [51] V. Kornich, C. Kloeffel, and D. Loss, Phonon-assisted relaxation and decoherence of singlet-triplet qubits in Si/SiGe quantum dots, *Quantum* **2**, 70 (2018).
- [52] X. Mi, M. Benito, S. Putz, D. M. Zajac, J. M. Taylor, G. Burkard, and J. R. Petta, A coherent spin-photon interface in silicon, *Nature* **555**, 599 (2018).
- [53] J. R. Petta, H. Lu, and A. C. Gossard, A Coherent Beam Splitter for Electronic Spin States, *Science* **327**, 669 (2010).
- [54] S. Nadj-Perge, S. M. Frolov, J. W. W. Van Tilburg, J. Danon, Y. V. Nazarov, R. Algra, E. P. A. M. Bakkers, and L. P. Kouwenhoven, Disentangling the effects of spin-orbit and hyperfine interactions on spin blockade, *Phys. Rev. B* **81**, 2 (2010).
- [55] S. Nadj-Perge, V. S. Pribiag, J. W. Van Den Berg, K. Zuo, S. R. Plissard, E. P. Bakkers, S. M. Frolov, and L. P. Kouwenhoven, Spectroscopy of spin-orbit quantum bits in indium antimonide nanowires, *Phys. Rev. Lett.* **108**, 1 (2012).
- [56] A. Zarassi, Z. Su, J. Danon, J. Schwenderling, M. Hovevar, B. M. Nguyen, J. Yoo, S. A. Dayeh, and S. M. Frolov, Magnetic field evolution of spin blockade in Ge/Si nanowire double quantum dots, *Phys. Rev. B* **95**, 1 (2017).